Composite Materials and Engineering, *Vol. 3, No. 3 (2021) 221-239*
https://doi.org/10.12989/cme.2021.3.3.221

Micro-CT image-based reconstruction algorithm for multiscale modeling of Sheet Molding Compound (SMC) composites with experimental validation

Hyoung Jun Lim[1], Hoil Choi[1], Sang-Jae Yoon[2], Sang Won Lim[2], Chi-Hoon Choi[2] and Gun Jin Yun*[1,3]

[1]*Department of Aerospace Engineering, Seoul National University, Seoul, 08826, South Korea*
[2]*Research & Development Division, Hyundai Motor Company, Gyeonggi, 18280, South Korea*
[3]*Institute of Advanced Aerospace Technology, Seoul National University, Seoul, 08826, South Korea*

(Received July 29, 2021, Revised September 28, 2021, Accepted December 17, 2021)

Abstract. This paper presents a multiscale modeling method for sheet molding compound (SMC) composites through a novel bundle packing reconstruction algorithm based on a micro-CT (Computed Tomography) image processing. Due to the complex flow pattern during the compression molding process, the SMC composites show a spatially varying orientation and overlapping of fiber bundles. Therefore, significant inhomogeneity and anisotropy are commonly observed and pose a tremendous challenge to predicting SMC composites' properties. For high-fidelity modeling of the SMC composites, the statistical distributions for the fiber orientation and local volume fraction are characterized from micro-CT images of real SMC composites. After that, a novel bundle packing reconstruction algorithm for a high-fidelity SMC model is proposed by considering the statistical distributions. A method for evaluating specimen level's strength and stiffness is also proposed from a set of high-fidelity SMC models. Finally, the proposed multiscale modeling methodology is experimentally validated through a tensile test.

Keywords: composite materials; finite element method; multiscale modeling; reconstruction algorithm; sheet molding compound;

1. Introduction

Carbon-fiber sheet molding compound (CF-SMC) composites receive increasing attention due to their huge potential in lightweight automotive, shipbuilding, power plant, and aerospace applications (Wilkinson and Ryan 1998, Lu *et al*. 2005, Cabrera-Ríos and Castro 2006). SMC composites have a good balance between mechanical performance, formability, and manufacturing costs compared with other composites. SMC composites have been applied in structural components, especially in the automobile field, such as external panels, trunk floors, and body subframes.

A compression molding process is utilized for the structural components (Abrams and Castro 2003, Görthofer *et al*. 2019, Meyer *et al*. 2020). The initial charge, which is the preform of the SMC

*Corresponding author, Professor, E-mail: gunjin.yun@snu.ac.kr

http://www.techno-press.org/?journal=cme&subpage=7 ISSN: 2671-4930 (Print), 2671-5120 (Online)

composites, comprises carbon-fiber bundles and resin matrix. And then, it is compressed into the shape of the final product. Due to the complex flow pattern during the compression molding process, the final molded parts show a spatially varying distribution of fiber bundles. Therefore, significant inhomogeneity and anisotropy are commonly observed and pose a tremendous challenge to predicting SMC composites' behavior in virtual tests (i.e., computational simulation).

Numerous researches have been conducted on multiscale modeling approaches for short-fiber reinforced composites to account for these features of the SMC composites. The homogenization method is critically important to estimate the effective properties of micro/mesostructure. In a multiscale analysis, analytical and computational homogenization techniques are frequently utilized to obtain effective properties. The micromechanics-based analytical homogenization method has been developed based on Eshelby's theory, for example, the self-consistent and Mori-Tanaka methods (Eshelby and Peierls 1957, Doghri and Ouaar 2003, Doghri *et al*. 2011, Lim *et al*. 2020). However, due to their limitations in simulating local damage occurrence in the microstructure, they are mainly used to simulate effective macroscopic behavior. There are various attempts to predict the mechanical properties of SMC composites through this technique. Anagnostou *et al*. (2018) adopted the hierarchical Mori-Tanaka scheme through a two-step homogenization. They firstly homogenized effective properties from the microstructure of the fiber bundle. After that, the macroscopic behavior of SMC composites was calculated through the second homogenization from the mesostructure. This hierarchical approach evaluated the effective viscoelastic behavior of fiber bundles and SMC plates by accounting for the time dependence. Görthofer *et al*. (2020) investigated the influence of the microstructural parameters through a sensitivity analysis. The parameters include the elastic moduli, volume fraction of the constituents, and the orientation of fiber. They figured out which parameters have a strong influence on overall behavior by constructing a heatmap. Recently, Tamboura *et al*. (2020) proposed the multiscale approach to predict the stiffness reduction of SMC composites subjected to low cycle fatigue. By considering the local cyclic normal and shear stress at the interface, the fiber-matrix interface damage criterion was introduced in the Mori-Tanaka method to predict the loss of stiffness. Although proven to be successful in predicting macroscale behavior through many studies, this analytical method still has a limitation in capturing local phenomena from a micro-scale point of view. Thus, it cannot express spatial variation and uncertainty in micro/mesostructure.

At present, the finite element (FE)-based computational method defining the representative volume element (RVE) has become promising to predict composites' behavior accurately. The CT(Computed Tomography)-based high fidelity RVE generation can reflect the characteristics of the microstructure in the most accurate way (Yu *et al*. 2017, Fládr *et al*. 2019, Lim *et al*. 2020, Lim *et al*. 2021). However, SMC composites have a more complex mesostructure unlike simple micro or mesostructures such as cross-ply laminate composites and particulate composites. Therefore, many attempts have been made to create statistically equivalent RVEs. For example, Li *et al*. (2018) studied a Voronoi diagram-based algorithm for modeling SMC mesostructures where each Voronoi cell corresponds to a fiber bundle with a distinct orientation. Next, using an algorithm of the random sequential adsorption (RSA), Chen *et al*. (2018) developed a framework for modeling SMC RVE based on a sequential bundle packing algorithm. They modeled the SMC fiber bundles by sequentially packing layer-by-layer, accounting for overlap between bundles through a rise and sink methodology. This method can efficiently reflect the features of SMC composites having high volume fraction and bent shape of the fiber bundle. However, they only considered the bundles' orientation from an averaged orientation tensor, first introduced by Advani and Tucker (1987). More information is required for advanced high-fidelity modeling of the SMC composites.

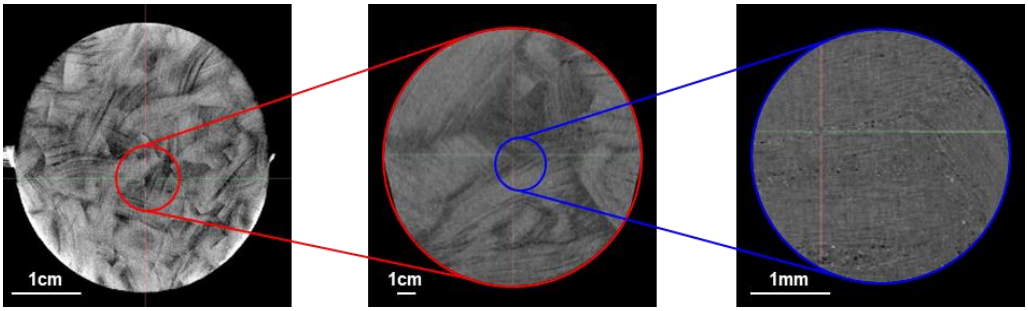

Fig. 1 Micro-CT in-plane images of SMC composites with different magnifications

This paper presents a micro-CT image processing and a novel bundle packing reconstruction algorithm to predict the mechanical properties of SMC composites. The orientation and dispersion of the fibers are characterized through micro-CT image processing. Because the only orientation-based SMC modeling yields relatively monotonic results in modulus and strength, it is necessary to improve the heterogeneous high-fidelity SMC modeling (Kravchenko *et al*. 2019, Sommer *et al*. 2020, Tang *et al*. 2020). Therefore, the dispersion of fibers is also considered in the reconstruction modeling. This idea comes from Kim and Yun (2018), which demonstrated the change in mechanical properties according to the dispersion of inclusion in particle-reinforced composites through principal component analysis (PCA). After that, a novel bundle packing reconstruction algorithm for a high-fidelity SMC model is introduced based on the manufacturing setup and image processing input parameters. Multiscale modeling is also presented to bridge mechanical properties from microscale to meso and macroscale. Finally, the proposed multiscale modeling is validated through comparison with the experimental test and discussed based on the results thoroughly.

2. Micro-CT image processing for statistical characterization of mesostructure

Micro-CT test is performed using Xradia 620 Versa (Carl Zeiss, USA) equipment. The statistical distributions of the fibers' orientation and local volume fraction are obtained from micro-CT images because they correlate with the mechanical properties (Kim and Yun 2018). Fig. 1 shows the in-plane micro-CT images with different magnifications. The micro-CT images are composed of several stack images. The samples with a diameter 40 mm and thickness 3 mm are extracted at the center of the SMC plate. The enlarged images show that the longitudinal fibers in the fiber bundles have no curvature. In the series of CT images, it is hard to distinguish the individual fiber bundles. The segment in the image processing is conducted in the scope of microscopic constituents: fiber and matrix.

2.1 Statistical distribution of fiber orientation

In this section, the gradient method is utilized to obtain the orientation of fibers by calculating the grayscale change in the images (Miletić *et al*. 2020). Image processing procedures are performed using MATLAB Image Processing Toolbox and consist of three steps. First, the histogram equalization is conducted to distinguish the fiber from the matrix in the micro-CT image. By this pre-processing step, the accuracy of the gradient method is improved. After that, the gradient method is applied to the pre-processed micro-CT image. In this step, a MATLAB built-in function

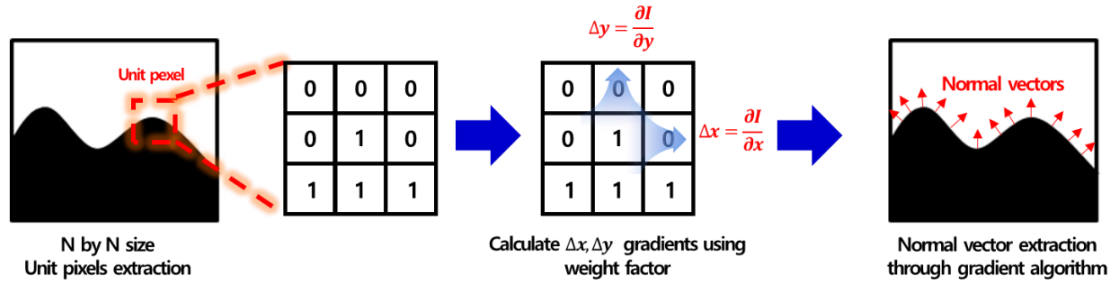

Fig. 2 Procedures of calculating the normal vector

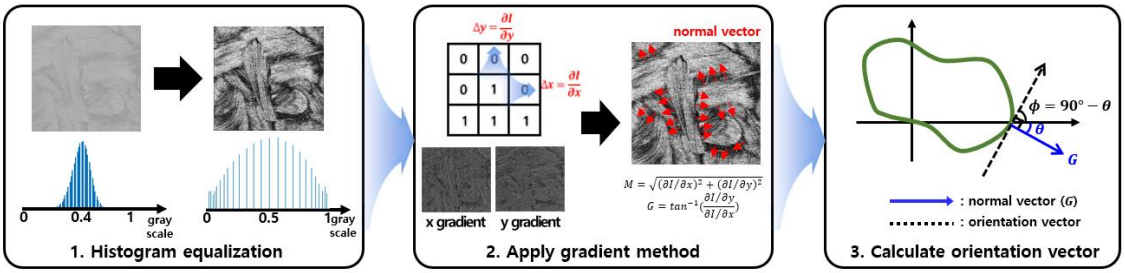

Fig. 3 Overall image processing procedures: Calculation of the fiber orientation

'imgradient' is used. Grayscale values of 3 by 3 pixels around the particular pixel are called from the micro-CT image to calculate the magnitude and normal vector at a specific pixel. Then, the image gradient (∇I) and the gradient orientation are computed based on the change of grayscale values (∂I) of X and Y-axis for each pixel (∂x, ∂y). M and G represent the magnitude and orientation of the image gradient calculated by Eq. (1). Through this operation, the magnitude and normal vector value of each pixel are computed. Detailed procedures of the gradient method are described in Fig. 2.

$$\nabla I = [\partial I/\partial x \quad \partial I/\partial y]^{\mathrm{T}}, \qquad M = \sqrt{(\partial I/\partial x)^2 + (\partial I/\partial y)^2}, \qquad G = tan^{-1}(\frac{\partial I/\partial y}{\partial I/\partial x}) \tag{1}$$

Finally, the orientation vector is calculated through the normal vector value by the gradient method. Overall image processing procedures to obtain fiber orientation are shown in Fig. 3.

2.2 Statistical distribution of fiber local volume fraction

The fiber local volume fraction is defined and computed using an image processing algorithm to evaluate the non-uniform distribution of the fibers in the SMC plate. First, the histogram equalization is performed as in the gradient method. Next, an image binarization is performed to differentiate between fiber and matrix. The grayscale value of the fiber and matrix was set to one and zero, respectively. In order to obtain statistical distribution data of the fiber local volume fraction, 1000 local sampling points & areas are randomly generated for each 2D micro-CT image. After that, the local fiber volume fraction in each sampling area is calculated to generate the distribution. In this case, the sampling area was set as a square with a side length of 200 pixels. The image processing procedures of calculating the local fiber volume fraction are summarized in Fig. 4.

The orientation and local volume fraction distribution are summarized in Fig. 5. Fig. 5(a) is the

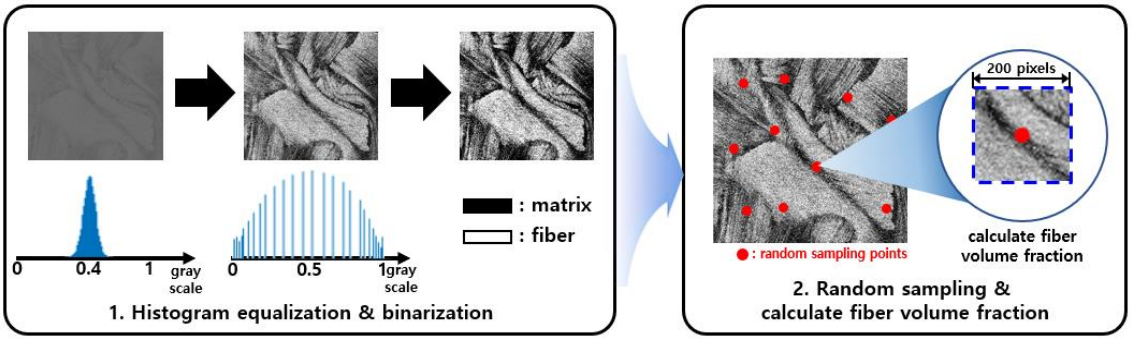

Fig. 4 Computation procedures of the local volume fraction at randomly preset sample points

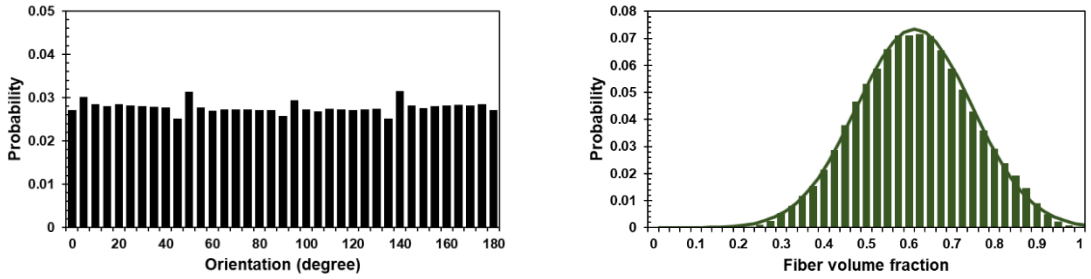

(a) (b)

Fig. 5 Statistical distributions from micro-CT image processing: (a) Orientation (b) local volume fraction

orientation distribution in the probability density function (PDF). It has uniform probabilities at every angle, indicating that the SMC composites have randomly oriented bundles. Fig. 5(b) exhibits the local volume fraction distribution. It has a shape of Gaussian distribution with the COV = 0.133. The fiber volume fraction from the micro-CT image processing is 55%, set as input quantity. The distributions of the orientation and local volume fraction are directly utilized in the reconstruction algorithm to generate high-fidelity SMC models.

3. A multiscale modeling of sheet molding compound for FE analysis

3.1 Input parameters and bundle repository

Through bundle packing, a novel reconstruction algorithm is developed to generate high-fidelity SMC models in a voxelated square space. For the reconstruction algorithm, manufacturing-dependent parameters are selected as inputs. It includes the sizes of the bundles and the plates, the bundle volume fraction, and the targeted statistical distributions of the bundles' orientation and local volume fraction. Among the input parameters, the targeted statistical distributions of bundles' orientation and local volume fraction in cumulative distribution function (CDF) are from micro-CT images. Statistical distribution of the bundle local volume fraction within a preset domain is determined from the prescribed random sample points. The sample points are prescribed randomly at the beginning of the algorithm. These locations of sample points do not change during the reconstruction algorithm. Thus, the distribution of the local volume fraction changes depending on

Table 1 List of the input parameters for the proposed SMC reconstruction algorithm

Classification		Symbol
The initial charge setup	Plate size	L_{plate}
	Number of the layers in the plate	n_{layer}
	Length of the bundle	L_{bundle}
	Width of the bundle	W_{bundle}
	The volume fraction of the bundles	V_{bundle}
The compression molding	Orientation of bundles	$F_{ori}(x)$
	The local volume fraction of bundles	$F_{local}(x)$

the location of bundle packing. The input parameters are summarized in Table 1 by classifying them into two.

Before bundle packing, the pre-processing is performed to build a repository of bundles based on the targeted orientation statistical distribution, as shown in Fig. 6. The number of bundles is computed in terms of SMC plate size, bundle sizes and the volume fraction of the bundles. In Eq. (2), NB_{layer} and NB_{plate} denote the number of bundles in a layer and plate, respectively

$$NB_{layer} = \left[\frac{L_{plate}^2 V_{bundle}}{W_{bundle} L_{bundle}}\right], \qquad NB_{plate} = NB_{layer} \cdot n_{layer} \tag{2}$$

3.2 Modified-RSA based stochastic reconstruction algorithm

The random sequential adsorption (RSA) algorithm for a multi-layer voxelated system is utilized (Feder 1980, Pan *et al*. 2008, Zhou *et al*. 2016). The RSA method sequentially packs arbitrary objects into space at random locations while avoiding overlapping until a desired number of objects are packed or a pre-specified iteration number is reached. The RSA-based reconstructed models have been widely used for composite modelings, such as short fiber reinforced composites (Pan *et al*. 2008, Luchoo *et al*. 2011, Zhao *et al*. 2020). The modified RSA algorithm presented by Chen *et al*. (2018) was utilized to express the undulation between fiber bundles. It dynamically moves the bundle segments to upper and lower layers to increase space utilization. Based on the input parameters in Section 3.1, fiber bundles are packed into a unit layer of the SMC plate. As a result, 3D SMC plates can be modeled by piling up multiple bundle-packed layers. There are two conditions in the bundle packing process in order to mimic the actual geometry of composites.

The first condition is to check the location feasibility of the bundles during the bundle packing process. Compared to the conventional RSA algorithm, in which overlapping is not allowed, the proposed packing algorithm is modified so that bundles can intersect at one location maximally. This restriction on the number of overlaps is because bundles tend to be uniformly distributed when compressing the initial charge of SMC composites. Additionally, if the allowable amount of overlapping has too much in the modeling, the SMC composites' shape could be distorted due to a bias of bundles' location.

Second, the local volume fraction of the SMC is calculated at the prescribed random sample points during the bundle packing process. It is repeatedly compared with the local volume fraction's targeted statistical distribution, whether it is within the tolerance range. Otherwise, a candidate of the bundle location would be altered and newly checked the conditions from the first condition.

Table 2 Pseudocode for bundle packing reconstruction algorithm

Numerical implementation	
Input: L_{plate}, L_{bundle}, n_{layer}, $F_{local}(x)$, $F_{ori}(x)$, V_{bundle}, W_{bundle}	
Output: 3D reconstructed model, the local orientations of bundles	
1	***for*** i = 1: n_{layer}
2	Initialize internal variables and start to pack fiber bundles on the (i)-th layer
3	Define random sample points for the local volume fraction
4	***while*** $\left\|V_{bundle}^{target} - V_{bundle}^{(i)}\right\| \leq tol$
5	Build fiber bundle repository using Eq. (2) and $F_{ori}(x)$.
6	***for*** j = 1: NB_{layer}
7	Define the bundle location: (x_{bundle}, y_{bundle})
8	***if*** location feasible
9	overlapped parts: pack on the (i+1)-th layer
10	overhanging parts: pack on the (i)-th layer
11	***else*** not feasible
12	go to line 7
13	***end if***
14	Calculate the local volume fraction distribution of (i)-th layer: $F_{local}^{(i)}(x)$
15	***if*** $\left\|F_{local}^{(i)} - F_{local}\right\| \leq tol$
16	continue the packing
17	***else***
18	cancel the packing and go to line 7
19	***end if***
20	***end for***
21	Calculate the volume fraction on the (i)-th plate: $V_{bundle}^{(i)}$
22	***end while***
23	Check the orientation distribution with the target
24	***end for***
25	Stacking up the reconstructed layers

During the bundle packing process, the calculated distribution of the local volume fraction has to be lower than the targeted CDF. Therefore, the relocation of a bundle occurs only when a value (probability) in a specific range (bin) of the CDF is larger than the corresponding targeted CDF value.

If these two conditions are satisfied, the bundle packing is conducted on the layer. A rise and sink process is applied during the bundle packing to represent the undulation by raising the overlapping parts to the upper layer. On the other hand, the overhanging parts of the bundle sink to the current layer. It is noted that this process creates the bent geometries of the bundles. As a result, the proposed bundle packing reconstruction algorithm can reflect physical features accurately. Finally, a computational procedure for the bundle packing reconstruction algorithm is summarized as Pseudocodes in Table 2. The overall flow chart is also depicted in Fig. 6.

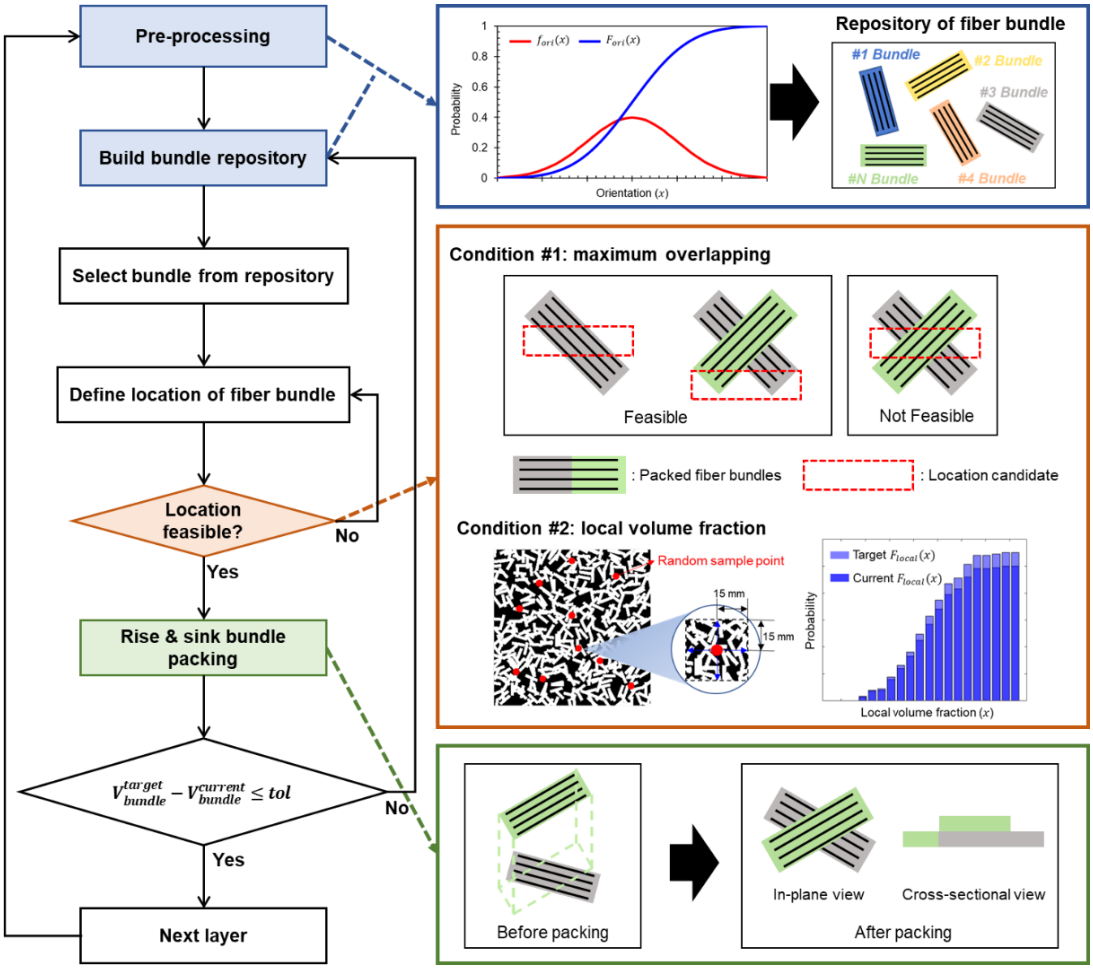

Fig. 6 A flow chart of bundle packing SMC reconstruction algorithm

The proposed reconstruction algorithm generates more realistic high-fidelity SMC models based on the direct statistical distributions of the orientation and local volume fraction. The proposed algorithm holds apparent advantages over the existing SMC modeling, which matches only the orientation of the bundle with an averaged orientation tensor (Chen *et al*. 2018). The input parameters in Table 3 are employed to create the single-layer SMC models using the proposed reconstruction algorithm. The statistics of bundles' orientation and the local volume fraction are generated through the Gaussian distribution by adjusting the mean and coefficient of variation (COV). First, Fig. 7 shows the reconstructed SMC models generated by varying the mean and COV of different orientations and assuming a uniform local volume fraction.

Fig. 7 shows that the reconstructed models change the trends of bundles' direction according to the mean values of the Gaussian distribution. COV values can control the randomness of fiber bundles. Fig. 8 exhibits the reconstructed models according to the local volume fraction's distribution. The volume fraction and orientation of the fiber bundle are assumed to be 55% and random, respectively. Reconstructed models are generated by varying the COV values of the local volume fraction distribution. When the COV is 0.1, it has a relatively uniform dispersion. In the

Table 3 The input parameters for the SMC reconstruction algorithm

Description	Value
Plate size	$300\text{mm} \times 300\text{mm}$
Bundle size	$25\text{mm} \times 5mm$
The volume fraction of the bundle	55%

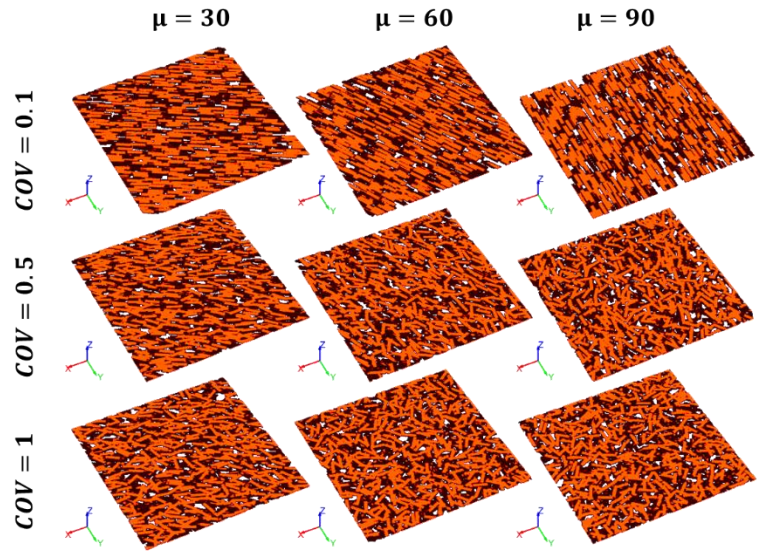

Fig. 7 Reconstructed models in different orientations with Gaussian distribution: μ (mean), COV (coefficient of variation)

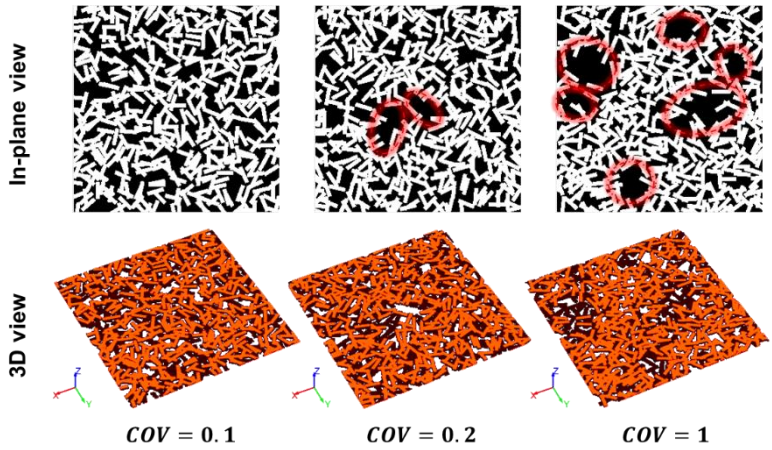

Fig. 8 Reconstruction models in different dispersions with Gaussian distribution: void **(**red circle)

case of more than 0.2, voids with large sizes are generated within the SMC plate. Further increment of the COV makes more voids resulting in highly biased bundle distributions.

By changing the statistical parameters of the proposed reconstruction algorithm, multiple layers of the SMC composites are generated. The high-fidelity SMC model is composed in the 3D

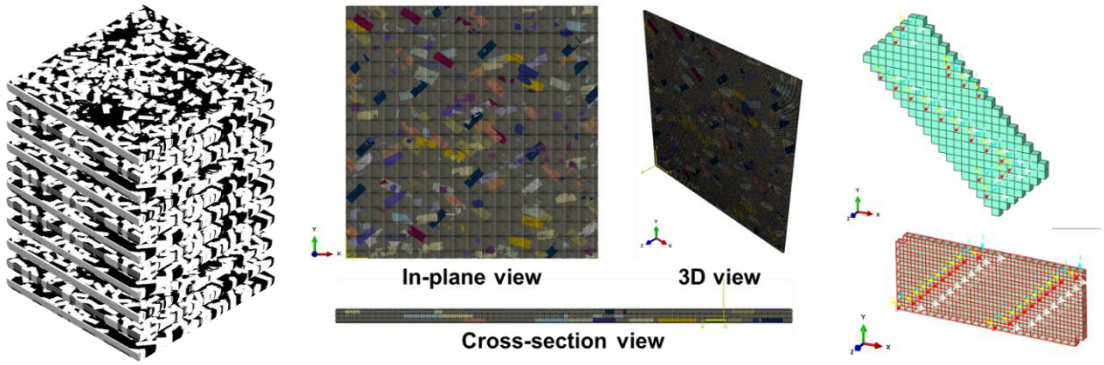

(a) (b) (c)

Fig. 9 FE modeling from reconstruction model: (a) Stack of SMC reconstructed models (b) C3D8 FE models with different views (c) Defining the local orientation for fiber bundles

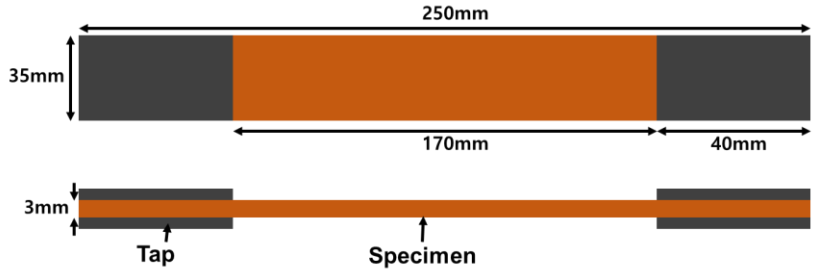

Fig. 10 Dimensions of a tensile specimen

voxelated cuboid space by stacking up the reconstructed layers. The voxels in the reconstruction model are converted into a solid element for FE simulation. Moreover, since each bundle is aligned at a specified angle, the elements corresponding to the bundle have a local orientation. In this study, nodes and connectivity of a C3D8 element are created according to Abaqus/Standard input format. All the process for FE modeling is depicted in Fig. 9.

4. Experimental validation of the SMC stiffness and strength

4.1 Tensile testing

An experimental tensile test is performed to obtain the mechanical properties of SMC composites. An initial charge with $200\text{mm} \times 200\text{mm}$ is subjected to a compression molding process to fabricate the SMC composites plate with a size of $300\text{mm} \times 300\text{mm} \times 3\text{ mm}$. The fiber bundles in the SMC plate have a quasi-isotropic orientation as observed in the micro-CT image processing. Tensile specimens are extracted from the molded plate with a 35mm width following the ASTM D3039. Considering the size of the fiber bundle, the specimen is designed to have a large enough width. Dimensions of the tensile specimen are depicted in Fig. 10. Sandpapers are attached to 40mm long grip regions at both ends of the specimens to prevent slipping during the testing. Therefore, the gage length of the tensile specimen becomes 170mm. From trimming the boundary

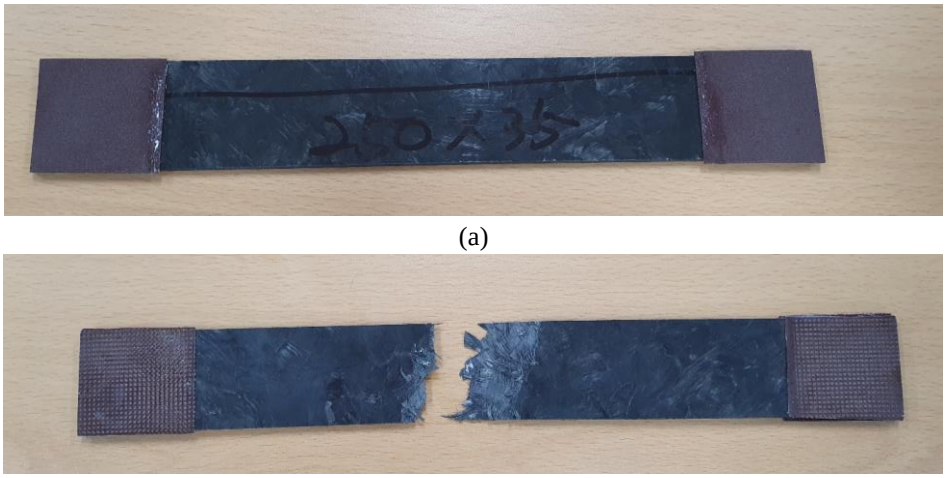

(a) (b)

Fig. 11 Experimental tensile specimens: (a) before testing (b) after testing

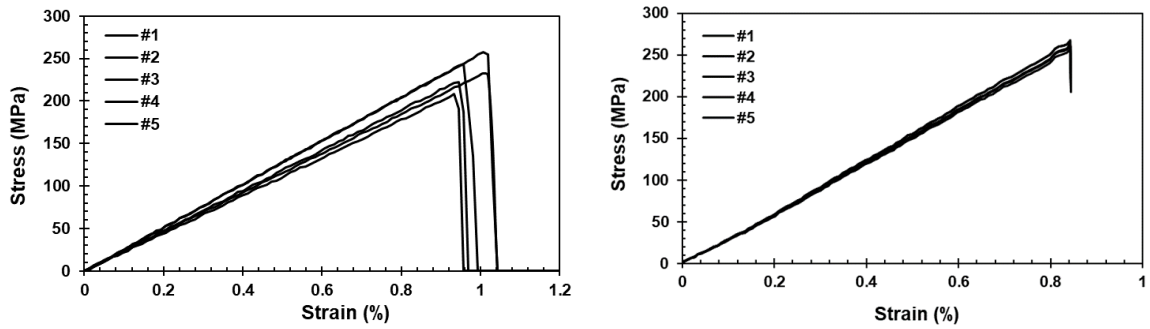

(a) (b)

Fig. 12 Stress-Strain curves from experiments: (a) Crosshead-based strain (b) DIC-based strain

of specimens, five specimen samples are prepared. The displacement-controlled uniaxial tensile test is performed with a 30 kN MTS material test machine with a 2 mm/min crosshead rate. The tensile specimens' photographs before and after testing are shown in Fig. 11. After failure, as shown in Fig. 11(b), it is observed that the matrix failure is dominant in the SMC specimen because the fiber bundles have their geometry even after specimen breakage. This failure pattern was also reported in the SMC composites' study (Martulli *et al*. 2019).

The experimental tensile tests are conducted by Seoul national university (SNU) and Hyundai motors group, with different strain measurement methods. In SNU, the strain is measured by dividing the crosshead displacement by the gage length of the tensile specimen. On the other hand, the average strain on the specimen surface using digital image correlation (DIC) equipment in the Hyundai motors group is measured. It is noted that the different strains are estimated depending on the strain measurement techniques (Motra *et al*. 2014). Generally, the crosshead strain is significantly greater than the DIC measurement. As a result, the crosshead-based modulus underestimates compared with the DIC-based measurement. The stress-strain curves are plotted in Fig. 12. Notably, because of the heterogeneity of the SMC composites, the difference in results

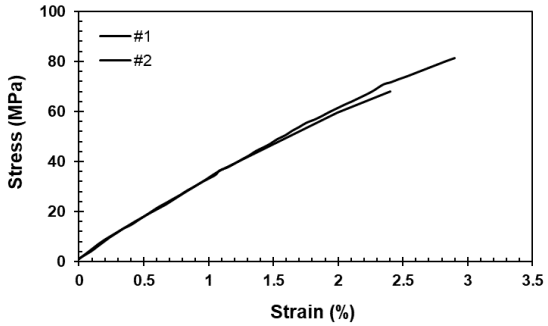

Fig. 13 Stress-strain curve of pure vinyl-ester resin from the tensile experimental test

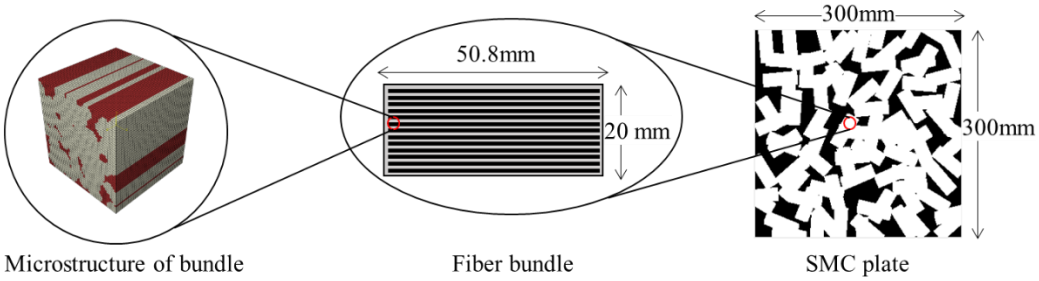

Fig. 14 Multiscale modeling of the SMC composites

between the two measurement techniques becomes more salient. Both stress-strain curves show linear behavior. The nominal stress is computed by dividing the force by the cross-sectional area of the tensile specimen. The elastic modulus is calculated by the curve's initial slope and measured in the 0.05 to 0.25% strain range. Likewise, the strength is measured based on ultimate maximum strength, which is the maximum stress of the stress-strain curve.

Fig. 13 shows the stress-strain curves of pure vinyl-ester resin from the tensile test. The vinyl-ester resin is utilized as the matrix in the SMC composites. The properties are employed in the simulation.

4.2 Tensile specimen modeling and measurement

Uniaxial tensile simulations are conducted with the reconstructed SMC models. The SMC plate and fiber bundle size are designed to have $300\ \text{mm} \times 300\ \text{mm} \times 3\ \text{mm}$ and $50.8\ \text{mm} \times 20\ \text{mm}$, respectively. The fiber volume fraction in the SMC plate is 55%, as revealed from micro-CT image processing. Therefore, the fiber bundle is assumed to comprise 78% fiber, and a unit layer is assumed to have a 70% fiber bundle volume fraction to match to 55% fiber volume fraction by $70\% \times 78\% = 55\%$.

The microstructure of the fiber bundle is shown in Fig. 14. The computational homogenization technique is required to obtain the effective properties of the fiber bundle. The details on the computational homogenization refer to the previous works (Zhu *et al*. 2018, Choi *et al*. 2019, Jeong *et al*. 2019). The microscale RVE with unidirectional fibers is shown in Fig. 14. The constituents are T700 carbon fiber and vinyl-ester resin. The mechanical properties of the constituents are from

Table 4 Mechanical properties of SMC composites

	T700	Vinyl-ester	Bundles' effective properties
E_1 (MPa)	240000	3480	203292
E_2 (MPa)	14700		11639
G_{12} (MPa)	6400		5027
G_{23} (MPa)	5400		4206
ν_{12}	0.3	0.3	0.01737
ν_{23}	0.35		0.349

literature and experimental tests (Martulli *et al*. 2018). The mechanical properties of constituents and the effective properties are summarized in Table 4.

The reconstruction algorithm uses the statistical distributions from micro-CT image processing to generate an SMC model with a 70% bundle volume fraction. As a result, a series of reconstructed layers are obtained, as shown in Fig. 15(a). After that, Fig. 15(b) shows that tensile specimens are extracted from the reconstructed SMC model. A total of 15 tensile specimens are prepared from the five reconstructed SMC models. A coupling constraint is applied to elements at both ends of the specimen with reference points for the tensile simulation. After that, boundary and loading conditions are applied to the reference points that correspond with the parts of grip and fixture in the tensile testing system, as shown in Fig. 15(c).

For strain measurement in the tensile simulation, two different methods are performed. The first is to measure the strain based on the crosshead displacement. Like the experiment, the strain from the simulation is obtained by dividing displacement by the gage length. The calculations of uniaxial strain and stress are expressed in Eq. (3).

$$\varepsilon_1 = \frac{u^*}{L_{gage}}, \qquad \sigma_1 = \frac{RF_1}{wt} \tag{3}$$

The second strain measurement method is by the digital image correlation (DIC) equipment. The effective strain is calculated by applying the volume-averaging scheme in terms of strain fields after tensile simulation. Although DIC is measured only on the surface of the specimen, the volume-averaging in simulations can be performed over the entire specimen domain. It is because of obtaining a more averaged strain in the specimen. The equation can be expressed as Eq. (4).

$$\varepsilon_1 = \frac{\int_\Omega \hat{\varepsilon}_1 d\Omega}{\int_\Omega d\Omega}, \qquad \sigma_1 = \frac{RF_1}{wt} \tag{4}$$

Herein, Ω is the total element domain of the specimen. This domain does not include the jig parts, which is also not ROI in the DIC measurement. $\hat{\varepsilon}_1$ is the uniaxial strain value at Gaussian points. With different types of strain measurement, the comparison of tensile modulus can be achieved with experimental results.

4.3 Experimental validation

Static finite element analysis is performed on the reconstructed SMC models subjected to tensile loading. Based on the strain mentioned above and stress measurements, the modulus of the SMC

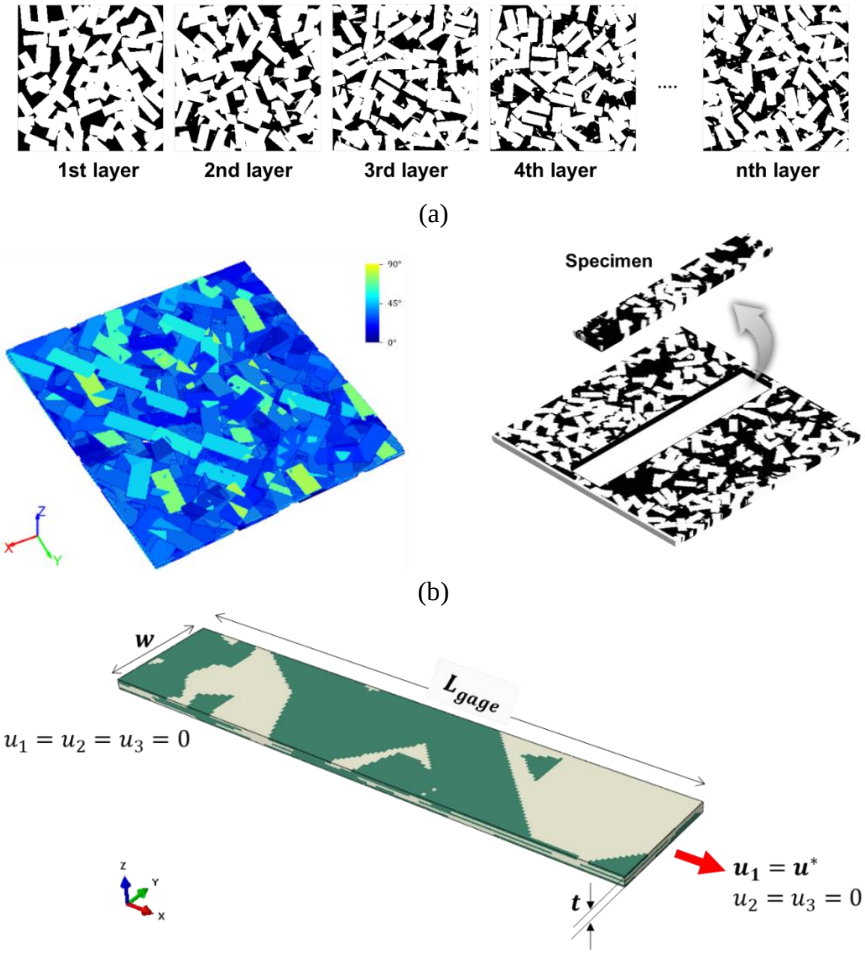

Fig. 15 High-fidelity SMC modeling: (a) Reconstructed models for each layer (b) orientation contour and specimen extraction (c) boundary condition for tensile test

Table 5 Mean and COV of elastic modulus with different number of layers (unit: GPa)

	5 layers		**7 layer**		**10 layers**		**13 layers**		**15 layers**	
	Crosshead	DIC	Crosshead	DIC	Crosshead	DIC	Crosshead	DIC	Crosshead	DIC
Mean	20.2	31.6	21.2	34.5	30.5	48.5	33.3	54.7	35.6	57.3
COV	0.26	0.37	0.22	0.25	0.16	0.17	0.14	0.14	0.12	0.13

composites is calculated from the initial slope of the stress-strain curve. Fig. 16 shows the modulus change according to the number of layers constituting the ASTM 3039 specimen with 3 mm thickness. Increment of the SMC modulus is observed in thinner layers in both strain measurement methods, as shown in Table 5. It is because of the increasing heterogeneity of the SMC mesostructure through the thickness. The deformation in the Z-direction due to the different properties of constituents occurs significantly during the tensile simulation. Thus, increasing the number of layers

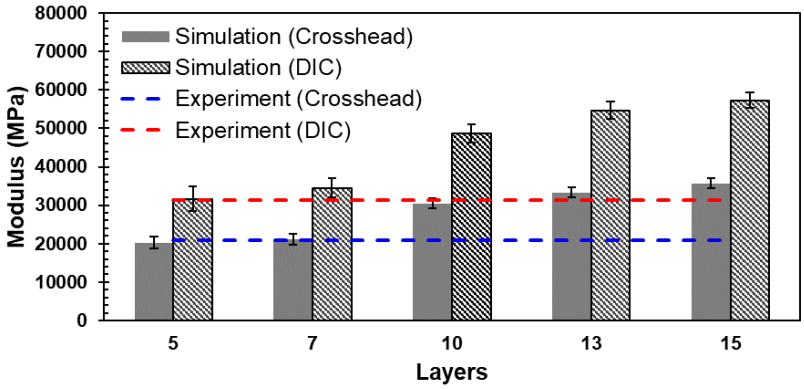

Fig. 16 Effect of the number of layers on the tensile modulus

improves the stress transfer between layers in the Z-direction and makes the SMC specimen stiffer. These investigations have also been handled in the literature to ensure the mechanical performance of SMC composites (Feraboli *et al*. 2009, Kravchenko *et al*. 2019). In addition, as the number of layers increases, the quasi-isotropy seems to increase, increasing the uniformity in the local volume fraction and orientation with the reduced sample-to-sample variability in effective properties. Despite the same statistical parameters, the different mesostructures between reconstructed models are obtained. Therefore, simulations make such variability denoted by a standard error in the graph.

Comparing with the experiments, both crosshead and DIC measurements seem to fit well with experimental tests in the case of 5~7 layers. Since carbon fiber tows have $200\sim300\ \mathrm{g/m^2}$ fiber areal weight (FAW), they are assumed to have a $0.2\ \mathrm{mm}\sim0.3\ \mathrm{mm}$ thickness. From the bundle thickness, the ideal lamination in the fiber bundles could be 10~15 layers for 3 mm specimen thickness when the resin is excluded. However, the number of layers becomes 5.5~8.25 when applied 55% fiber volume fraction to the number of the ideal lamination. Therefore, it is validated that the prediction with tensile simulation has a good agreement with experimental results.

Next, a method is introduced for predicting tensile strength through the FE static simulation. The tensile strength of SMC composites is mainly dependent on the matrix based on the existing reports and our inspection of failure patterns in Fig. 11 (Martulli *et al*. 2019). Therefore, this study proposes that the strength of the SMC composite is predicted based on the matrix strength. In the previous section, the vinyl-ester resin has a strength of 65~80 MPa from tensile tests. An assumption is made that failure of SMC composites yields when the volume-averaged stress of the matrix region in the simulation models reaches the pure vinyl-ester's strength from the experimental test. The volume-averaged stress of the matrix region is computed as follows.

$$\sigma_{Matrix} = \frac{\int_{\Omega_{Matrix}} \hat{\sigma}_1 d\Omega_{Matrix}}{\int_{\Omega_{Matrix}} d\Omega_{Matrix}} \tag{5}$$

The volume-averaged stress in the matrix region is calculated when the uniaxial stress level of the specimen calculated in Eq. (3) reaches 260MPa, the tensile strength from the experimental tests. Fig. 17 shows the volume-averaged stress of the matrix for the different number of layers at the moment of reaching the experimental strength (260MPa). It is noted that decreasing the matrix volume-averaged stress with the increasing number of layers implies the decreasing load-carrying

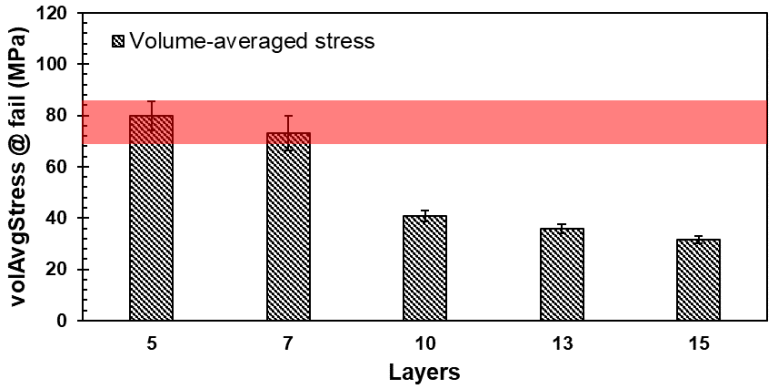

Fig. 17 Volume average stress in the matrix region for the number of layers (red band: strength from the experiment)

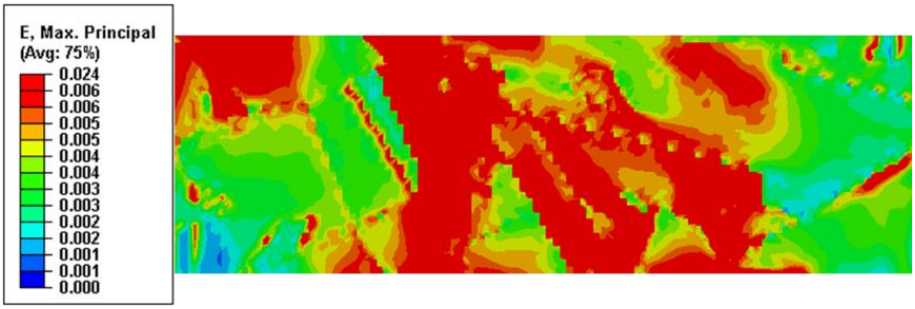

(a)

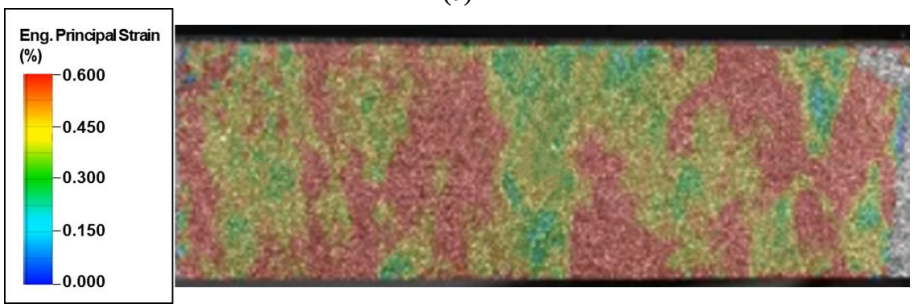

(b)

Fig. 18 Engineering principal strain contours: (a) SMC simulation (b) DIC measurement.

by the matrix and increasing load-carrying by the fiber bundles. The higher modulus of the SMC specimen with the increasing number of layers, as shown in Fig. 16, seems to be attributed to this mechanism. The red band in Fig. 17 represents the range of pure resin strength from the experimental test. The matrix volume-averaged stress from the simulation matches with the experimental strength with 5~7 layers. This match sufficiently supports the proposed strength evaluation method using the high-fidelity SMC composite models. In Fig. 18, the heterogeneous strain distribution can be identified in the simulation, which is also observed in the experiment. It shows the influence of the spatially varying distribution of fiber bundles. In conclusion, it is demonstrated that the proposed

SMC reconstruction algorithm can directly reflect the mesostructure of the actual SMC composites, and also, the proposed strength and stiffness evaluation method can accurately predict the mechanical properties of actual SMC composites.

5. Conclusions

This paper proposed a novel multiscale modeling method for SMC composites using micro-CT image processing procedures and a novel bundle packing reconstruction algorithm. Different measurement techniques were adopted when predicting the SMC composites' elastic modulus and successfully validated the prediction against the experimental results. Furthermore, the prediction of SMC composites' strength and modulus through static FE simulations are investigated, and the following conclusions are made:

• The micro-CT image processing was presented to obtain statistical distributions for the fiber bundle orientation and local volume fraction.

• The reconstruction algorithm can efficiently generate high-fidelity SMC models directly utilizing the targeted statistical distribution from micro-CT image processing of actual specimens.

• Experimental tensile tests were conducted, and corresponding FE simulations were demonstrated.

• The effect of the number of layers in the predictions of strength and modulus of actual specimens was discussed, and the comparison was successfully conducted with experimental results measured differently: crosshead-based and DIC-based.

• The strength prediction for SMC composites was proposed based on the volume-averaged stress in the matrix region and had a good agreement with experimental results.

Acknowledgments

The research was supported by Hyundai Motors Co. Ltd (No. 0498-20200036) and the Institute of Engineering at Seoul National University. The authors are grateful for their support.

References

Abrams, L.M. and Castro, J.M. (2003), "Predicting molding forces during sheet molding compound (SMC) compression molding. I: Model development", *Polym. Compos.*, **24**(3), 291-303. https://doi.org/10.1002/pc.10029.

Advani, S.G. and Tucker, C.L. (1987), "The use of tensors to describe and predict fiber orientation in short fiber composites", *J. Rheol.*, **31**(8), 751-784. https://doi.org/10.1122/1.549945.

Anagnostou, D., Chatzigeorgiou, G., Chemisky, Y. and Meraghni, F. (2018), "Hierarchical micromechanical modeling of the viscoelastic behavior coupled to damage in SMC and SMC-hybrid composites", *Compos. Part B Eng.*, **151**, 8-24. https://doi.org/10.1016/j.compositesb.2018.05.053.

Cabrera-Ríos, M. and Castro, J.M. (2006), "An economical way of using carbon fibers in sheet molding compound compression molding for automotive applications", *Polym. Compos.*, **27**(6), 718-722. https://doi.org/10.1002/pc.20257.

Chen, Z., Huang, T., Shao, Y., Li, Y., Xu, H., Avery, K., Zeng, D., Chen, W. and Su, X. (2018), "Multiscale finite element modeling of sheet molding compound (SMC) composite structure based on stochastic mesostructure reconstruction", *Compos. Struct.*, **188**, 25-38. https://doi.org/10.1016/j.compstruct.2017.12.039.

Choi, H.I., Zhu, F.Y., Lim, H. and Yun, G.J. (2019), "Multiscale stochastic computational homogenization of the thermomechanical properties of woven Cf/SiCm composites", *Compos. Part B Eng.*, **177**, 107375. https://doi.org/10.1016/j.compositesb.2019.107375.

Doghri, I., Brassart, L., Adam, L. and Gérard, J.S. (2011), "A second-moment incremental formulation for the mean-field homogenization of elasto-plastic composites", *Int. J. Plasticity*, **27**(3), 352-371. https://doi.org/10.1016/j.ijplas.2010.06.004.

Doghri, I. and Ouaar, A. (2003), "Homogenization of two-phase elasto-plastic composite materials and structures: Study of tangent operators, cyclic plasticity and numerical algorithms", *Int. J. Solid Struct.*, **40**(7), 1681-1712. https://doi.org/10.1016/S0020-7683(03)00013-1.

Eshelby, J.D. and Peierls, R.E. (1957), "The determination of the elastic field of an ellipsoidal inclusion, and related problems", *Proceedings of the Royal Society of London. Series A. Mathematical and Physical Sciences*, **241**(1226), 376-396. https://doi.org/10.1098/rspa.1957.0133.

Feder, J. (1980), "Random sequential adsorption", *J. Theor. Biol.*, **87**(2), 237-254. https://doi.org/10.1016/0022-5193(80)90358-6.

Feraboli, P., Peitso, E., Deleo, F., Cleveland, T. and Stickler, P.B. (2009), "Characterization of prepreg-based discontinuous carbon fiber/epoxy systems", *J. Reinf. Plast. Comp.*, **28**(10), 1191-1214. https://doi.org/10.1177/0731684408088883.

Fládr, J., Bílý, P. and Broukalová, I. (2019), "Evaluation of steel fiber distribution in concrete by computer aided image analysis", *Compos. Mater. Eng.*, **1**(1), 49-70. https://doi.org/10.12989/cme.2019.1.1.049.

Görthofer, J., Meyer, N., Pallicity, T.D., Schöttl, L., Trauth, A., Schemmann, M., Hohberg, M., Pinter, P., Elsner, P., Henning, F., Hrymak, A., Seelig, T., Weidenmann, K., Kärger, L. and Böhlke, T. (2019), "Virtual process chain of sheet molding compound: Development, validation and perspectives", *Compos. Part B Eng.*, **169**, 133-147. https://doi.org/10.1016/j.compositesb.2019.04.001.

Görthofer, J., Schneider, M., Ospald, F., Hrymak, A. and Böhlke, T. (2020), "Computational homogenization of sheet molding compound composites based on high fidelity representative volume elements", *Computat. Mater. Sci.*, **174**, 109456. https://doi.org/10.1016/j.commatsci.2019.109456.

Jeong, S., Zhu, F., Lim, H., Kim, Y. and Yun, G.J. (2019), "3D stochastic computational homogenization model for carbon fiber reinforced CNT/epoxy composites with spatially random properties", *Compos. Struct.*, **207**, 858-870. https://doi.org/10.1016/j.compstruct.2018.09.025.

Kim, Y. and Yun, G.J. (2018), "Effects of microstructure morphology on stress in mechanoluminescent particles: Micro CT image-based 3D finite element analyses", *Compos. Part A Appl. S.*, **114**, 338-351. https://doi.org/10.1016/j.compositesa.2018.08.033.

Kravchenko, S.G., Sommer, D.E., Denos, B.R., Favaloro, A.J., Tow, C.M., Avery, W.B. and Pipes, R.B. (2019), "Tensile properties of a stochastic prepreg platelet molded composite", *Compos. Part A Appl. S.*, **124**, 105507. https://doi.org/10.1016/j.compositesa.2019.105507.

Li, Y., Chen, Z., Su, L., Chen, W., Jin, X. and Xu, H. (2018), "Stochastic reconstruction and microstructure modeling of SMC chopped fiber composites", *Compos. Struct.*, **200**, 153-164. https://doi.org/10.1016/j.compstruct.2018.05.079.

Lim, H., Choi, H., Lee, M.J. and Yun, G.J. (2020), "Elasto-plastic damage modeling and characterization of 3D needle-punched Cf/SiCm composite materials", *Ceram. Int.*, **46**(10), 16918-16931. https://doi.org/10.1016/j.ceramint.2020.03.271.

Lim, H.J., Choi, H., Lee, M.J. and Yun, G.J. (2021), "An efficient multi-scale model for needle-punched Cf/SiCm composite materials with experimental validation", *Compos. Part B Eng.*, **217**, 108890. https://doi.org/10.1016/j.compositesb.2021.108890.

Lim, H.J., Choi, H., Zhu, F.Y., Kerekes, T.W. and Yun, G.J. (2020), "Multiscale damage plasticity modeling and inverse characterization for particulate composites", *Mech. Mater.*, **149**, 103564. https://doi.org/10.1016/j.mechmat.2020.103564.

Lu, J., Khot, S. and Wool, R.P. (2005), "New sheet molding compound resins from soybean oil. I. Synthesis and characterization", *Polymer*, **46**(1), 71-80. https://doi.org/10.1016/j.polymer.2004.10.060.

Luchoo, R., Harper, L.T., Warrior, N.A. and Dodworth, A. (2011), "Three-dimensional numerical modelling of discontinuous fibre composite architectures", *Plast. Rubber Compos.*, **40**(6-7), 356-362.

https://doi.org/10.1179/1743289810Y.0000000023.
Martulli, L.M., Alves, M., Pimenta, S., Hine, P.J., Kerschbaum, M., Lomov, S.V. and Swolfs, Y. (2018). "Predictions of carbon fibre sheet moulding compound (CF-SMC) mechanical properties based on local fibre orientation", *Proceedings ECCM 18*, *18th European Conference on Composite Materials*, Athens, Greece, June.
Martulli, L.M., Muyshondt, L., Kerschbaum, M., Pimenta, S., Lomov, S.V. and Swolfs, Y. (2019), "Carbon fibre sheet moulding compounds with high in-mould flow: Linking morphology to tensile and compressive properties", *Compos. Part A Appl. S.*, **126**, 105600. https://doi.org/10.1016/j.compositesa.2019.105600.
Meyer, N., Schöttl, L., Bretz, L., Hrymak, A.N. and Kärger, L. (2020), "Direct bundle simulation approach for the compression molding process of sheet molding compound", *Compos. Part A Appl. S.*, **132**, 105809. https://doi.org/10.1016/j.compositesa.2020.105809.
Miletić, M., Kumar, L.M., Arns, J.Y., Agarwal, A., Foster, S.J., Arns, C. and Perić, D. (2020), "Gradient-based fibre detection method on 3D micro-CT tomographic image for defining fibre orientation bias in ultra-high-performance concrete", *Cement Concrete Res.*, **129**, 105962. https://doi.org/10.1016/j.cemconres.2019.105962.
Motra, H.B., Hildebrand, J. and Dimmig-Osburg, A. (2014), "Assessment of strain measurement techniques to characterise mechanical properties of structural steel", *Eng. Sci. Technol., Int. J.*, **17**(4), 260-269. https://doi.org/10.1016/j.jestch.2014.07.006.
Pan, Y., Iorga, L. and Pelegri, A.A. (2008), "Analysis of 3D random chopped fiber reinforced composites using FEM and random sequential adsorption", *Computat. Mater. Sci.*, **43**(3), 450-461. https://doi.org/10.1016/j.commatsci.2007.12.016.
Pan, Y., Iorga, L. and Pelegri, A.A. (2008), "Numerical generation of a random chopped fiber composite RVE and its elastic properties", *Compos. Sci. Technol.*, **68**(13), 2792-2798. https://doi.org/10.1016/j.compscitech.2008.06.007.
Sommer, D.E., Kravchenko, S.G., Denos, B.R., Favaloro, A.J. and Pipes, R.B. (2020), "Integrative analysis for prediction of process-induced, orientation-dependent tensile properties in a stochastic prepreg platelet molded composite", *Compos. Part A Appl. S.*, **130**, 105759. https://doi.org/10.1016/j.compositesa.2019.105759.
Tamboura, S., Ayari, H., Shirinbayan, M., Laribi, M.A., Bendaly, H., Sidhom, H., Tcharkhtchi, A. and Fitoussi, J. (2020), "Experimental and numerical multi-scale approach for Sheet-Molding-Compound composites fatigue prediction based on fiber-matrix interface cyclic damage", *Int. J. Fatigue*, **135**, 105526. https://doi.org/10.1016/j.ijfatigue.2020.105526.
Tang, H., Chen, Z., Xu, H., Liu, Z., Sun, Q., Zhou, G., Yan, W., Han, W. and Su, X. (2020), "Computational micromechanics model based failure criteria for chopped carbon fiber sheet molding compound composites", *Compos. Sci. Technol.*, **200**, 108400. https://doi.org/10.1016/j.compscitech.2020.108400.
Wilkinson, A.N. and Ryan, A.J. (1998), *Polymer Processing and Structure Development*, Springer, Netherlands.
Yu, J., Zhou, C. and Zhang, H. (2017), "A micro-image based reconstructed finite element model of needle-punched C/C composite", *Compos. Sci. Technol.*, **153**, 48-61. https://doi.org/10.1016/j.compscitech.2017.09.029.
Zhao, J., Su, D.X., Yi, J.M., Cheng, G., Turng, L.S. and Osswald, T. (2020), "The effect of micromechanics models on mechanical property predictions for short fiber composites", *Compos. Struct.*, **244**, 112229. https://doi.org/10.1016/j.compstruct.2020.112229.
Zhou, J., Qi, L. and Gokhale, A.M. (2016), "Generation of three-dimensional microstructure model for discontinuously reinforced composite by modified random sequential absorption method", *J. Eng. Mater. Technol.*, **138**(2), 021001. https://doi.org/10.1115/1.4032152.
Zhu, F.Y., Jeong, S., Lim, H.J. and Yun, G.J. (2018), "Probabilistic multiscale modeling of 3D randomly oriented and aligned wavy CNT nanocomposites and RVE size determination", *Compos. Struct.*, **195**, 265-275. https://doi.org/10.1016/j.compstruct.2018.04.060.